PROCEEDINGS OF SCIENCE

Observation of Clouds characteristics over the Eastern Tibetan Plateau

Nan Bai[a] **and Fengrong Zhu**[a,b,*]

[a] *School of Physical Science and Technology, Southwest Jiaotong University 611756, Chengdu, China*
[b] *School of Science, Xizang University, 850001, Lhasa, China*

E-mail: bainan@my.swjtu.edu.cn, zhufr@home.swjtu.edu.cn

Clouds are closely related to weather and serve as a key factor in Earth's climate system. Over the Tibetan Plateau (TP), cloud variations significantly impact radiation budgets and the global water cycle. This study examines cloud characteristics at the Large High Altitude Air Shower Observatory (LHAASO) site using CL51 ceilometer data (October 2020-June 2022) and CloudSat-CALIPSO data (2010-2019), analyzing cloud occurrence frequency (COF), cloud vertical structure (CVS), including cloud base height (CBH) and cloud layer stratification, while assessing MERRA-2 reanalysis data performance. Results show comparable COF between ground-based (43.7%) and satellite measurements (44.9%), with nighttime (October-May, 20:00-05:00 Beijing time) frequency averaging 34.2% and reaching its minimum at midnight. Distinct seasonal patterns emerge, showing maximum CBH in summer and minimum in winter. Single-layer clouds dominate the region, with summer and autumn exhibiting pronounced unimodal vertical structures, while spring and winter display more uniform distributions. MERRA-2 accurately represents high-level clouds but significantly underestimates mid- and low-level clouds. Both observation methods detect frequent cloud occurrence around 1 km, though satellite data reveals an additional peak near 5 km. These findings provide critical cloud data for climate dynamics and weather process studies over the Tibetan Plateau, improve cloud parameterization in climate models, and offer valuable operational references for LHAASO wide field of view Cherenkov telescope observations.

39th International Cosmic Ray Conference (ICRC2025)
15–24 July 2025
Geneva, Switzerland

ICRC 2025
The Astroparticle Physics Conference
Geneva July 15-24, 2025

*Speaker

PoS(ICRC2025)456

1. Introduction

Clouds are critical components of Earth's weather systems and climate dynamics. Their macroscopic properties—particularly cloud occurrence frequency (COF), cloud base height (CBH), and cloud vertical structure (CVS)—profoundly influence Earth's radiative balance by modulating atmospheric energy budgets and large-scale circulation through radiative feedbacks [1, 2]. For cosmic ray detection, cloud height also plays a critical role in measurement accuracy [3]. The Large High Altitude Air Shower Observatory (LHAASO) is situated on the eastern slope of the Tibetan Plateau (TP) —a region with a highly complex climate system where clouds significantly modulate both regional and global atmospheric circulation [4–6].

Investigating the macroscopic cloud characteristics in this region holds significant scientific and practical importance. Numerous studies have examined these cloud properties over the TP using various observational platforms. Previous research using CloudSat data shows a positive correlation between cloud radiative forcing and COF [7]. TP clouds display unique diurnal patterns: afternoon thermal forcing triggers convection [8], with a nighttime transition to stratiform precipitation. Geostationary satellite data reveal that COF peaks at 12:00 local standard time (LST) (with a minimum at 04:00 LST), a pattern that is consistent across subregions [9] . The plateau's topography compresses cloud layer thickness and cloud top height (CTH), while the CVS associated with precipitation intensity shows strong seasonal variations, including narrower CTH ranges in spring (around 12 km) compared to broader ranges in summer (12–18 km) [10]. Terrain-induced variations in COF and CVS highlight the need for regional studies [11].

The eastern slope of the TP features complex topography characterized by intersecting mountain ranges, where heavy precipitation events frequently occur. However, meteorological observations in this region remain limited due to the relatively short measurement history and sparse observational network. Consequently, ground-based investigations of cloud macroscopic characteristics have been rarely reported for this area. This study utilizes data from the Vaisala CL51 ceilometer (October 2020 to June 2022) combined with CloudSat-CALIPSO data (2010-2019) collected at LHAASO [12] on the TP, and evaluates the applicability of MERRA-2 reanalysis data. Through synergistic analysis of these datasets, we quantify the diurnal and seasonal variations of COF, CBH, and CVS at the LHAASO site. These results provide valuable observational constraints for understanding cloud processes over the TP's eastern slope while simultaneously offering practical guidance for LHAASO Wide Field Cherenkov Telescope Array (WFCTA) observations.

2. Data and Methods

LHAASO (29.35°N, 100.13°E, 4410 m above sea level) is located at Haizi Mountain in Daocheng County, Sichuan Province, China, on the eastern slope of the TP. Figure 1 shows the geographical location of the LHAASO station and the data screening coverage area. The observatory occupies approximately 1.3 km^2 of flat, open terrain with grassland-dominated vegetation.

2.1 CL51 Data

The Vaisala CL51 ceilometer uses short-pulse diode laser LIDAR technology to measure CBH with a maximum detection range of 15 km, height resolution of 10 m, and temporal resolution of

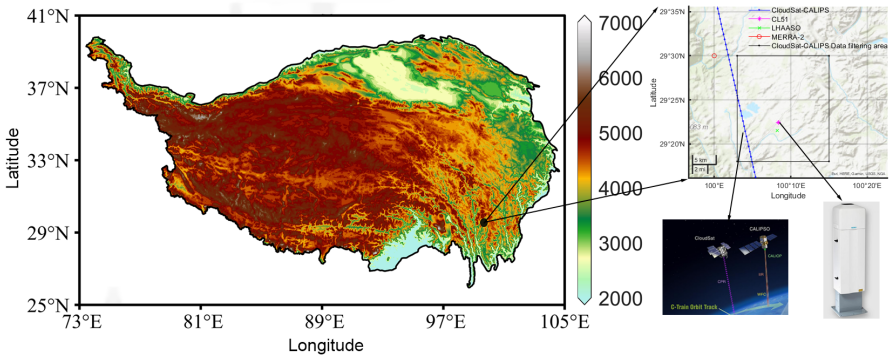

Figure 1: Topography of the TP with the location of the LHAASO observation site (29.35° N, 100.13° E, 4410 m above sea level), highlighting the study domain (black rectangle: 29.30-29.50°N, 100.05-100.25°E) for 2010-2019 CloudSat-CALIPSO (blue point) and MERRA-2 data(red circle) analysis. Photographs of the CL51 ceilometer and CloudSat-CALIPSO are also provided.

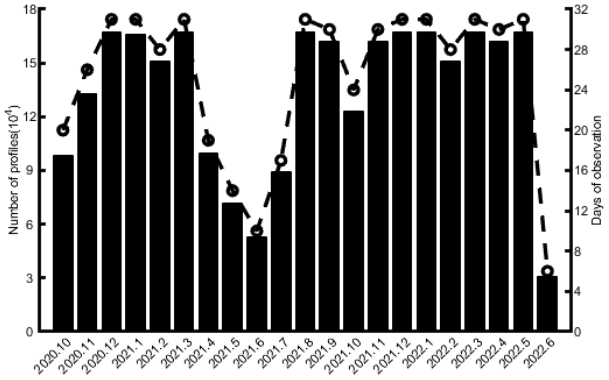

Figure 2: Number of profiles observed (column chart) and days with observation (line chart) of each month during the observation period.

16 s [13, 14]. Data from October 2020 to June 2022 were used (Figure 2), yielding 530 effective observation days with 2,824,497 valid detections. Quality control measures included eliminating data affected by precipitation, fog, or other non-penetrative conditions.

2.2 CloudSat-CALIPSO Data

CloudSat's 94 GHz millimeter-wave radar and CALIPSO's CALIOP lidar provide detailed cloud fraction and CBH data. This study uses CloudSat-CALIPSO 2B-GEOPROF-LIDAR data (2010-2019) from 515 overpasses within 29.30-29.50°N, 100.05-100.25°E. CBHs were converted to AGL values. Observations occurred at 03:00-04:00 and 14:00-15:00 Beijing Time due to the satellites' sun-synchronous orbit.

2.3 MERRA-2 Data

MERRA-2 (Modern-Era Retrospective Analysis for Research and Applications, Version 2), NASA's latest atmospheric reanalysis data (0.5°×0.625°, 3-hourly), provides aerosol and meteoro-

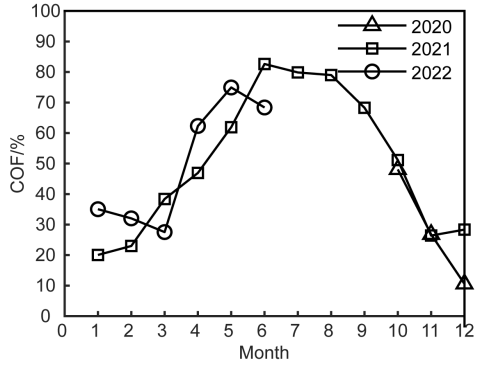

Figure 3: Cloud occurrence frequency (COF) of each month during the observation period form CL51.

logical assimilation data. This study uses 2010-2019 cloud fraction data from the grid point nearest LHAASO (29.5°N, 100°E).

3. Results

3.1 Cloud occurrence frequency

The COF is quantitatively defined as COF = (Number of times at least one cloud layer was detected/Total valid detections) × 100% [15–19], reflects the relative frequency of cloud presence over a given period. During the observation interval, the CL51 ceilometer measured a COF of 43.7%, while CloudSat-CALIPSO observations for 2010–2019 yielded a closely aligned COF of 44.9%, demonstrating consistency between ground- and satellite-based measurements. Given the CL51's substantially larger sample size, its data were prioritized for analyzing temporal variations in COF.

The LHAASO-WFCTA observation period spans from October to May of the following year. During this period, the nighttime COF (20:00–05:00 Beijing Time, same below) is 34.2%, peaking at its lowest around midnight (24:00). Because clouds absorb Cherenkov light, WFCTA observations should prioritize time slots with lower cloud coverage. Furthermore, cloud-free data should be selected during subsequent data screening. Thus, the impact of clouds on WFCTA data quality is significant and cannot be overlooked. These findings provide critical guidance for WFCTA operations and observations.

Seasonal COF variability is clearly demonstrated in Figure 3, based on CL51 measurements. The observed COF peaked at 82.6% in June 2021 (summer) and reached its minimum of 20.1% in January 2021 (winter). The data reveal a gradual COF increase from January to May, followed by a steady decrease from September to December. Notably, while September-October values remained consistent between 2020 and 2021, December 2020 showed significantly lower COF values. Furthermore, the 2022 trend diverged from the 2021 pattern, potentially attributable to monsoon variability or other climatic factors, highlighting the need for further analysis of atmospheric circulation patterns and thermodynamic conditions.

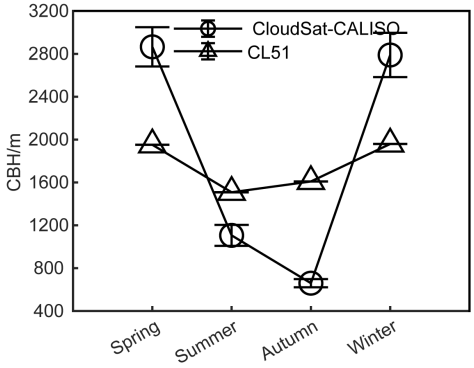

Figure 4: Seasonal distribution of mean height at cloud base height (CBH).

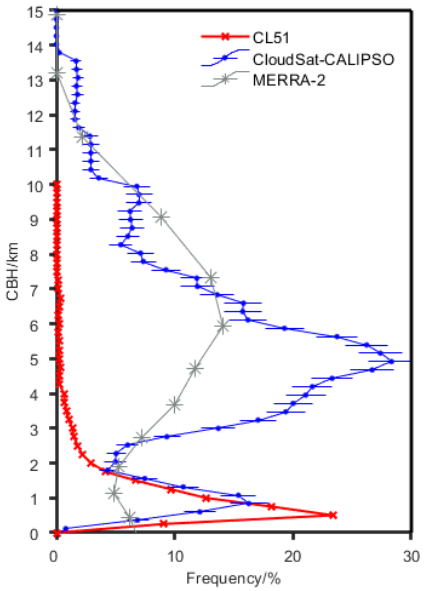

Figure 5: Distributions of CBHs by CL51, CloudSat-CALIPSO and MERRA-2.

3.2 Cloud vertical structure

CVS is primarily characterized by CBH, the COF of single-layer, multi-layer, and clustered cloud distributions, as well as the vertical spacing between CBHs [16, 19]. These parameters can be derived from the vertical CBH profile measured by the CL51. Clouds at different vertical levels modulate atmospheric circulation by altering the diabatic heating/cooling gradient [20].

At LHAASO, clear skies occurred 55% of the time versus 45% cloudy periods. Single-layer clouds dominated (81%), followed by double-layer (15%) and rare triple-layer clouds (1%). CBH comparisons (Figure 4) showed satellite-CL51 differences: satellites measured higher CBH in spring/winter but lower in summer/autumn. The CL51 observed the lowest summer CBH, while satellites showed autumn minima. Both agreed on the seasonal patterns, consistent with TP cloud variability [21].

Figure 5 shows CVS distributions from CL51, CloudSat-CALIPSO, and MERRA-2 data. Satellite observations reveal two CBH peaks, while MERRA-2 performs well for high clouds but significantly underestimates mid- and low-level clouds—consistent with Miao et al. [22]'s findings that MERRA-2 overestimates TP cloud heights. Unlike ground-based instruments, the primary peak in satellite data occurs at 5 km, whereas CL51 observations indicate that clouds most frequently appear at around 1 km in height and are less common above 2 km. Several factors may contribute to this discrepancy. First, when encountering thick cloud layers such as deep convective clouds, lidar struggles to penetrate them due to severe signal attenuation, leading to missed detections of upper-level clouds. Similarly, spaceborne lidar, which emits laser pulses downward, suffers from signal attenuation at lower altitudes, resulting in underdetection of low-level clouds. This explains why satellite data show a concentration of cloud at higher altitudes, while ground-based lidar observations exhibit the opposite trend. Therefore, combining both datasets provides a more comprehensive understanding of CVS. Additionally, since cloud structure is primarily influenced by topography and monsoon dynamics, we disregard the potential impact of differing observation periods between the two instruments in this analysis.

Figure 6 shows the monthly CBH distributions. Although the CVS during the observation period generally exhibited a unimodal pattern, distinct seasonal patterns emerge: in summer/autumn, clouds are concentrated below 2000 m, while spring/winter distributions are more uniform. Notable monthly variations are observed: April 2021 shows a bimodal structure, in contrast to April 2022's uniform peak at 400–800 m. In November, clouds generally remain below 2000 m, but in 2020, they extended up to 10,000 m with a uniform upper distribution. April 2022 exhibits extreme variability (1000–10,000 m), accompanied by heavy rainfall, suggesting the influence of frontal systems—consistent with the findings of Costa-Surós et al. [16] on frontal cloud dynamics.

4. Conclusions

This study investigates COF, CBH, and CVS at the LHAASO site on the eastern TP using Vaisala CL51 ceilometer data from October 2020 to June 2022 and CloudSat-CALIPSO data from 2010-2019, while evaluating the applicability of MERRA-2 reanalysis data for representing local CVS. The main findings are summarized as follows:

(1) CL51 and satellite COF measurements showed strong agreement (43.7% vs. 44.9%), with clear seasonal variation (summer maximum, winter minimum). This seasonal pattern primarily results from the combined effects of large-scale atmospheric circulation and local topographic forcing. During summer, the thermal low-pressure system over the plateau transports moisture from the Indian Ocean, which subsequently undergoes orographic lifting, leading to enhanced cloud formation and precipitation. In contrast, dry northeasterly winds from Siberia and Mongolia dominate during winter, resulting in reduced cloudiness. The nocturnal COF minimum (34.2% during 20:00–05:00 from October to May) provides a valuable reference for WFCTA observations.

(2) Seasonal comparisons show satellite-derived CBH is higher in winter/spring but lower in summer/autumn than ground measurements, though both agree on the seasonal pattern. Enhanced high clouds in spring/summer, consistent with ISCCP/MODIS data [19], result from intensified convection due to orographic lifting of Indian Ocean moisture and plateau thermal forcing.

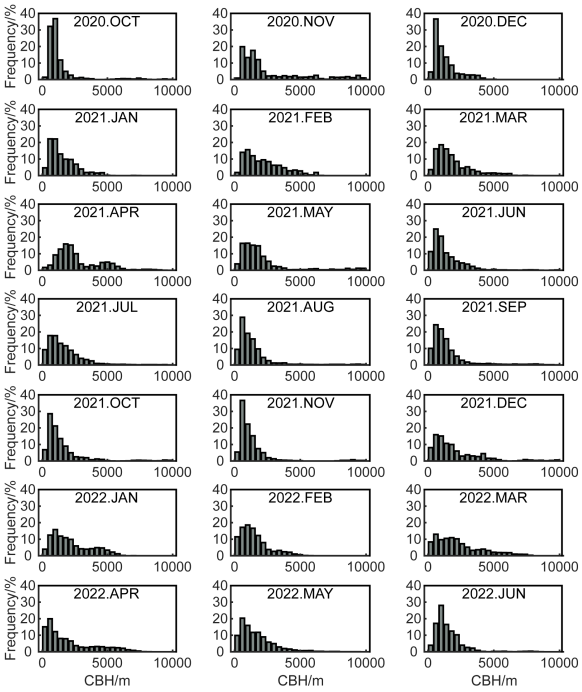

Figure 6: Cloud vertical structure of every month during CL51 observation period.

(3) MERRA-2 accurately captures high clouds but underestimates mid/low clouds. Satellite data show cloud peaks at 1 km and 5 km, while ground-based CL51 detects only the 1 km peak due to their different detection perspectives (top-down vs. bottom-up). Combining both methods offers a more complete CVS assessment.

References

[1] Stephens, G. L. Cloud Feedbacks in the Climate System: A Critical Review. *J. Clim.* **2005**, *18*, 237–273.

[2] Voigt, A.; Albern, N.; Ceppi, P.; Grise, K.; Li, Y.; Medeiros, B. Clouds, Radiation, and Atmospheric Circulation in the Present-Day Climate and under Climate Change. *WIREs Clim. Change* **2021**, *12*, e694.

[3] Cai, Y. P.; Luo, C. R.; Chen, S.; Wang, Z. S.; Lü, Q. Y.; Huang, P. Cloud Distribution Characteristics over the Southeastern Coastal Region of China Detected by Laser Ceilometer. *Meteorol. Mon.* **2023**, *49*, 170–177.

[4] Wu, G. X.; Liu, Y. M.; Wang, T. M.; Wan, R. J.; Liu, X.; Li, W. P.; Wang, Z. Z.; Zhang, Q.; Duan, A. M.; Liang, X.Y. The Influence of Mechanical and Thermal Forcing by the Tibetan Plateau on Asian Climate. *J. Hydrometeorol.* **2007**, *8*, 770–789.

[5] Yang, K.; Wu, H.; Qin, J.; Lin, C. G.; Tang, W. J.; Chen, Y. Y. Recent Climate Changes over the Tibetan Plateau and Their Impacts on Energy and Water Cycle: A Review. *Glob. Planet. Change* **2014**, *112*, 79–91.

[6] Tiwari, S.; Kar, S. C.; Bhatla, R. Dynamic Downscaling over Western Himalayas: Impact of Cloud Microphysics Schemes. *Atmos. Res.* **2018**, *201*, 1–16.
[7] Wei, J.; Duan, K. Q.; Xin, R. Characteristics of Cloud Occurrence Probability and Radiative Forcing over the Tibetan Plateau. *J. Glaciol. Geocryol.* **2020**, *42*, 368–377.
[8] Tang, J.; Guo, X. L.; Chang, Y. Numerical Simulation Study on Microphysical Characteristics of Clouds and Precipitation over the Tibetan Plateau in Summer 2014. *Acta Meteorol. Sin.* **2018**, *76*, 1053–1068.
[9] Xu, W. J.; Lü, D. R. Analysis of Cloud Distribution and Diurnal Variation over the Tibetan Plateau in Summer Based on Geostationary Satellite Observations. *Clim. Environ. Res.* **2023**, *28*, 229–241.
[10] Yan, Y. F.; Wang, X. C.; Liu, Y. M. Cloud Vertical Structures Associated with Precipitation Magnitudes over the Tibetan Plateau and Its Neighboring Regions. *Atmos. Ocean. Sci. Lett.* **2018**, *11*, 44–53.
[11] Chen, H. M.; Yuan, W. H.; Li, J.; Yu, R. C. A Possible Cause for Different Diurnal Variations of Warm Season Rainfall as Shown in Station Observations and TRMM 3B42 Data over the Southeastern Tibetan Plateau. *Adv. Atmos. Sci.* **2012**, *29*, 193–200.
[12] Cao, Z.; Chen, M. J.; Chen, S. Z.; Hu, H. B.; Liu, C.; Liu, Y.; Ma, L. L.; Ma, X. H.; Sheng, X. D.; Wu, H. R.; et al. Overview of the Large High Altitude Air Shower Observatory (LHAASO). *Acta Astron. Sin.* **2019**, *60*, 1–16.
[13] Wang, Y.; Zhao, C. F.; Dong, Z. P.; Li, Z. Q.; Hu, S. Z.; Chen, T. M.; Tao, F.; Wang, Y. Z. Improved Retrieval of Cloud Base Heights from Ceilometer Using a Non-Standard Instrument Method. *Atmos. Res.* **2018**, *202*, 148–155.
[14] Bai, Z. N.; Alaiyi, A. D.; Li, R. N.; et al. Comparative Analysis of Near-Infrared Laser Cloud Height Meter and Micro-Pulse Lidar. *Mod. Agric. Sci. Technol.* **2015**, *647*, 251–252, 255.
[15] Zhou, L. L.; Xu, G. R.; Wu, D. Q.; Liu, T. Comparative Analysis of Cloud Height Observations from Laser Ceilometer and Infrared Thermometer. *Torrential Rain Disasters* **2018**, *37*, 470–478.
[16] Costa-Surós, M., Calbó, J., González, J. A., Martin-Vide, J. Behavior of Cloud Base Height from Ceilometer Measurements. *Atmos. Res.* **2013**, *127*, 64–76.
[17] Poore, K. D.; Wang, J. H.; Rossow, W. B. Cloud Layer Thicknesses from a Combination of Surface and Upper-Air Observations. *J. Clim.* **1995**, *8*, 550–568.
[18] Rossow, W. B.; Schiffer, R. A. ISCCP Cloud Data Products. *Bull. Am. Meteorol. Soc.* **1991**, *72*, 2–20.
[19] Li, J. M.; Huang, J. P.; Yi, Y. H.; Lü, D. R. Statistical Characteristics of Cloud Vertical Distribution over East Asia Using Satellite-Borne Lidar Data. *Chin. J. Atmos. Sci.* **2009**, *33*, 689–707.
[20] Randall, D. A.; Harshvardhan; Dazlich, D. A.; Corsetti, T. G. Interactions among Radiation, Convection, and Large-Scale Dynamics in a General Circulation Model. *J. Atmos. Sci.* **1989**, *46*, 1943–1970.
[21] Li, D.; Liu, Y. Z.; Shao, T. B.; Luo, R.; Tan, Z. Y. Evaluation of ERA5 Cloud Base Height Products Using Ground-Based Observations. *Chin. J. Atmos. Sci.* **2024**, *48*, 735–744.
[22] Miao, H.; Wang, X. C.; Liu, Y. M.; et al. An evaluation of cloud vertical structure in three reanalyses against CloudSat/cloud-aerosol lidar and infrared pathfinder satellite observations. *Atmospheric Science Letters.* **2019**. *20*, e906.